ACS APPLIED MATERIALS & INTERFACES

Forum Article

www.acsami.org

Challenges in the Characterization of Plasma-Processed Three-Dimensional Polymeric Scaffolds for Biomedical Applications

Ellen R. Fisher*

Department of Chemistry, Colorado State University, Fort Collins, Colorado 80523-1872, United States

ABSTRACT: Low-temperature plasmas offer a versatile method for delivering tailored functionality to a range of materials. Despite the vast array of choices offered by plasma processing techniques, there remain a significant number of hurdles that must be overcome to allow this methodology to realize its full potential in the area of biocompatible materials. Challenges include issues associated with analytical characterization, material structure, plasma processing, and uniform composition following treatment. Specific examples and solutions are presented utilizing results from analyses of three-dimensional (3D) poly(ε-caprolactone) scaffolds treated with different plasma surface modification strategies that illustrate these challenges well. Notably, many of these strategies result in 3D scaffolds that are extremely hydrophilic and that enhance human Saos-2 osteoblast cell growth and proliferation, which are promising results for applications including tissue engineering and advanced biomedical devices.

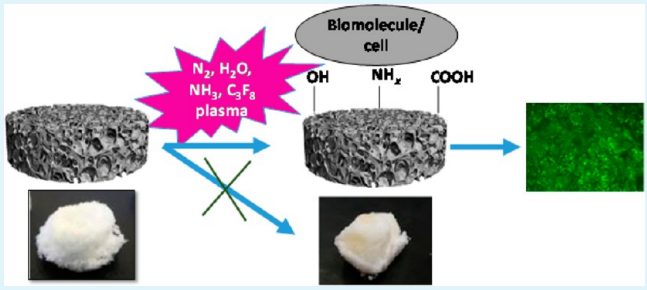

KEYWORDS: *3D polymeric scaffolds, biomaterials, plasma processing, surface modification, cell-surface interactions*

INTRODUCTION

Over the past few decades, many researchers have focused their attention on creating advanced materials for use in a range of biological systems and devices from directed drug delivery vehicles to artificial joints and tissues to biosensors.[1−5] The ability to tailor the surface functionality of a given substrate affords immense advantages in the construction of viable and long-lasting biomedical devices.[6] Indeed, for many devices, primary failure mechanisms are largely related to compatibility between the artificial material and surrounding tissues and/or biofluids.[7−9] Thus, the ability to strategically and specifically modify surface chemistry, topography (microstructure and nanostructure) and wettability without changing the bulk properties of the material continues to be the "holy grail" of biomaterials research.

Recently, researchers have focused on two biodegradable polymeric materials, poly(D,L-lactic acid) (PD,LLA) and poly(ε-caprolactone) (PCL)[10] to create three-dimensional (3D) scaffolds for a range of biomedical applications, most notably tissue engineering.[11−17] Although the 3D structure nominally mimics the structural design of the extracellular matrix, it is critical that any 3D construct used in the development of artificial tissues also have the surface properties that provide the appropriate biological responses from proteins, cells, and other biofluids.[17,18] One of the major drawbacks to using either PD,LLA or PCL for tissue regeneration is that these polymers are naturally hydrophobic, which tends to inhibit cell adhesion and proliferation. One approach to modifying PD,LLA and PCL is to graft extracellular matrix components such as proteins (e.g., fibronectin) or smaller peptide sequences onto the surface of the polymer scaffold.[6,17,19] The presence of such bioactive ligands into the polymer structure can enhance cell adhesion and function.

Plasma surface modification represents an extremely versatile approach to biomaterial modification as it allows for the precise tailoring of three important factors, surface chemistry, wettability, and morphology.[20−25] Plasma processing provides additional processing advantages including small processing costs, low waste, short processing time, and non-line-of-sight modification abilities for treatment of objects with complex geometries, such as those often found in biomedical devices. In general, two major plasma modification strategies have been employed. Functional group implantation (simply called surface modification) describes systems utilizing non-depositing precursors such as O_2, N_2, or H_2O to produce specific chemical functional groups ($-NH_x$, $-OH$, $-COOH$, etc.) on the surface of the 3D network. Alternatively, film deposition via plasma polymerization produces a thin film with the desired properties, ideally conformally coating the entire 3D structure without changing the mechanical properties of the material. A third method that has been employed, generally called plasma graft copolymerization,[26] entails exposing the polymer to an inert gas plasma (e.g., argon) to create radical sites in the surface. The activated surface can then be exposed to a polymerizing gas such as acrylamide, acrylic acid, or alkenes to create a thin polymeric layer.

Special Issue: New Frontiers and Challenges in Biomaterials

Received: July 1, 2013
Accepted: August 26, 2013
Published: September 12, 2013

   dx.doi.org/10.1021/am4025966 | *ACS Appl. Mater. Interfaces* 2013, 5, 9312−9321

Despite the vast array of choices offered by plasma processing techniques, there remains a significant number of hurdles that must be overcome to allow this methodology to realize its full potential in the area of 3D biocompatible materials. As detailed here, some of these challenges can be attributed to the materials (e.g., rough topography, nonuniform interconnectivity, and random pore size and distribution); some can be attributed to the plasma processes, which can impart nondesirable changes in the physical structure of the constructs; and some can be attributed to the complexity associated with characterizing the entire polymer network using appropriate compositional, morphological, and biological analyses. Here, 3D PCL scaffolds are treated with H_2O/N_2 and H_2O/NH_3 plasma modification and C_3F_8 plasma polymerization systems to illustrate these challenges. X-ray photoelectron spectroscopy (XPS), scanning electron microscopy (SEM), dynamic water contact angle (WCA) measurements, and cell response studies were used to characterize untreated and plasma processed materials. Notably, the specific systems discussed here show promise for creating tailored biomaterials with desirable surface properties to promote cell growth and proliferation, as exemplified by cell adhesion studies using human Saos-2 osteoblast cells.

EXPERIMENTAL DETAILS

Chemicals. Poly(ε-caprolactone), (PCL; molecular weight of M = 65 kDa), $CHCl_3$ (99%), absolute ethanol (99%) and NaCl (>99%) were purchased from Sigma–Aldrich (St. Louis, MO). The NaCl was sieved to a defined particulate size (150–300 μm diameter), using two 50- and 100-mesh screen sieves (Sigma–Aldrich). C_3F_8 (Airgas, 99.96%), N_2 (95%, Airgas; 99.999%, Air Liquid), NH_3 Matheson Tri-Gas, product grade), and deionized (DI) H_2O (18 Ω) were used for the plasma treatments. Prior to use, the liquid precursors underwent several freeze–pump–thaw cycles to remove dissolved gases.

Preparation of Polymer Scaffolds. PCL scaffolds were fabricated using a solvent casting/particulate leaching technique described previously.[15] Briefly, PCL pellets were dissolved in $CHCl_3$ (20/80 w/w) and allowed to sit in a sealed container for 2–4 h, forming a viscous, homogeneous solution. NaCl, the porogen, was incorporated into the PCL solution (5/95 w/w PCL/NaCl). The granular mixture was hand-pressed uniformly into the wells of Teflon molds (10 or 20 mm in diameter; 3 or 4 mm deep). The molded constructs dried for 1 h at room temperature, were immersed in ethanol for 3 h to allow phase separation and solvent evaporation, and immersed in DI water overnight to begin the leaching process. Individual samples were removed from the mold and immersed in fresh DI water for an additional 36–48 h to leach any remaining salt. During this period the water was replaced 2–3 times per day. Upon completion of the leaching period, the scaffolds were removed from the water and allowed to dry in air at room temperature for several days before use or were vacuum-dried overnight to speed the drying process. For aging experiments, after plasma treatment, samples were stored covered under ambient laboratory conditions.

Surface Modification of Scaffolds. Plasma surface modification was performed in one of two reactors. For the N_2/H_2O systems, a reactor designed from a borosilicate glass chamber 30 mm in diameter and 118 cm long was used. This reactor has been described in detail previously.[27] Gas pressure in the chamber was monitored using a Baratron capacitance manometer (MKS 626, 1 Torr). N_2 flow was controlled through an MKS mass-flow controller (20 sccm) and H_2O vapor was controlled via a needle valve. Total gas flow was maintained at 15 sccm; total reactor pressure was ~150 mTorr, and the treatment time was 4 min; applied rf power (P) was 30 W. Three different discharges were used: 100% water vapor (100% H_2O), 100% nitrogen (100% N_2), and a mixture of 50% N_2 and 50% H_2O (50/50 H_2O/N_2).

The second reactor, used for all other plasma treatments, was a 40-cm tubular-glass 13.56 MHz ICP plasma reactor, described previously.[28,29] Samples were placed on a substrate holder oriented parallel to the gas flow on the center axis of the reactor, either in the coil region of the reactor or at alternate locations downstream. MKS mass flow controllers and Nupro bellows sealed metering valves regulated the flow of gas precursors and vapor from liquid precursors, respectively. The total system pressure and partial pressures of each monomer gas were measured with an MKS Baratron capacitance manometer (1 Torr). Briefly, the following plasma conditions for H_2O/NH_3 plasmas were used: P = 30 W, total system pressure = 250 mTorr, and treatment time = 4–7 min. The following conditions were used for C_3F_8 plasmas: P = 50 W, total system pressure = 50 mTorr, and treatment time = 5–90 min, with substrates placed 15 cm downstream from the coil region of the reactor.

Characterization of Plasma-Treated Surfaces. Dynamic WCA measurements were performed with a KSV CAM 200 system to evaluate the change in WCA following plasma modification. For each sample, a 4-μL drop was placed on the scaffold; five measurements were made at different positions on the scaffold and averaged. In video capture mode, the camera acquired 400 frames at intervals of 6 ms. WCA and drop volume were measured and calculated using the instrument's software. The rate of absorption was measured in terms of rate of change in volume (V) of the water drop ($\Delta V/\Delta t$). Fitting the time dependent data to extract WCA values at t = 0 and the water absorption rate of the samples is discussed further in the next section.

XPS analysis was performed on PCL scaffolds using either a Theta Probe Thermo VG system or a Physical Electronics Model PE5800 ESCA/AES system. With both instruments, both electron (16–24 eV) and Ar-ion neutralizers were used for charge neutralization. Binding energies were charge corrected by setting the C_{1s} aliphatic carbon signal to 285.0 eV. C_{1s} peak fitting was performed using Thermo Scientific Avantage Data System software or XPSPEAK 4.1 software. In general, curve fitting was achieved using Gaussian functions with the full width at half maximum (FWHM) of each peak being ~2.0 eV, which is typical for plasma polymers.[29,30] Four components were used, with peaks centered at (1) 285.0 eV (C–C/C–H); (2) 286.5 ± 0.2 eV (C–OH/C–O–C); (3) 288.2 ± 0.2 eV (O–C–O/C═O); and (4) 289.1 eV (COOH/COOR), considering the chemical formula of PCL. After plasma modification with the nondepositing systems, two further components were added at 286.0 (C–N/C–O) and 288.0 eV (N–C═O). Additional details on fitting of XPS data are provided below.

SEM analysis (JEOL, Model JSM-6500F) was used to analyze scaffold surface morphology. An accelerating voltage of ≤15.0 kV and working distance of ≤10 mm were used for all analyses unless otherwise indicated. To analyze both chemical composition and morphology of the interior of the scaffolds, sections perpendicular or parallel to the scaffold top were made by freezing the scaffolds in liquid N_2 briefly (i.e., only 5–60 s) and then cutting with a scalpel blade.

Cell Behavior. Native and plasma-treated scaffolds were treated with human Saos-2 osteoblast cells (5.0×10^4 cells/scaffold) and allowed to culture for ~1, ~2, and ~5 days. Cell viability was determined by measuring the cell mitochondrial activity using the MTT colorimetric assay, which uses optical density as measured by UV/vis spectroscopy (λ = 570 nm) to evaluate the concentration of formazen crystals.[12] Cell morphology and spreading characteristics were analyzed with an Axiomat epifluorescence microscope (Zeiss, Germany). Prior to analysis, a 4% formaldehyde/PBS solution (300 °C) was used to fix the cells, which were then permeabilized with PBS containing 0.1% Triton X-100 and incubated with Alexa Fluor488 phalloidin (green fluorescence, Molecular Probes) for 20–30 min to visualize actin cytoskeleton. Images were made of both scaffold tops and cross sections.

RESULTS AND DISCUSSION

As noted in the Introduction, there are many challenges associated with accurate characterization of 3D biomaterials. Additional issues arise when these materials are plasma-treated to improve their surface properties for specific applications. Here, several of these challenges are discussed using both plasma surface modification (i.e., functional group implanta-

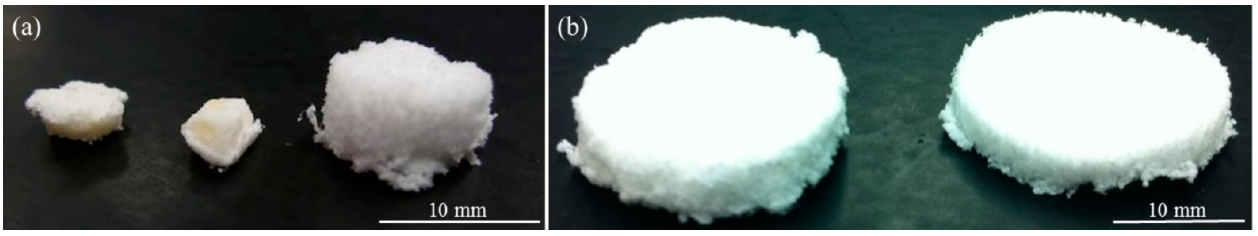

Figure 1. Photographs of (a) two 10-mm-diameter PCL scaffolds (left) that were treated in a 30 W N_2 plasma for 2 min 8 cm downstream from the coil region of the plasma, along with a 10-mm-diameter untreated PCL scaffold (far right); and (b) two 20-mm-diameter PCL scaffolds, one that was treated for 4 min in a rotating drum reactor using a 30 W, 50/50 H_2O/N_2 plasma (left) and an untreated scaffold (right).

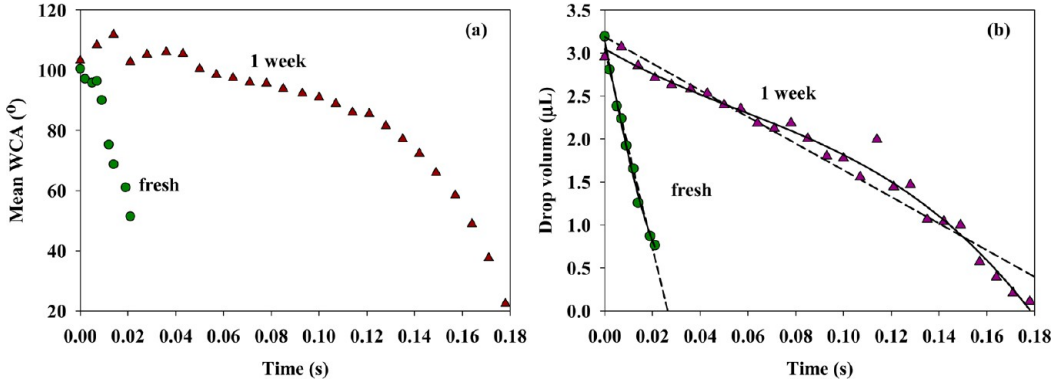

Figure 2. (a) Drop volume as a function of time for dynamic WCA measurements made on a PCL scaffold treated in a 50/50 H_2O/N_2 plasma at 30 W for 4 min (150 mTorr) measured immediately after treatment (green circles, labeled "fresh") and 1 week after treatment (red triangles, labeled "1 week"). Dashed lines represent linear regression analysis of the data, whereas solid lines are cubic polynomial fits to the data.

tion) and plasma polymerization (i.e., coating) of 3D PCL scaffolds as examples.

Plasma Damage. As is well-known in the plasma community, plasmas contain high densities of energetic particles that can interact with surfaces in undesirable ways. This presents an even more difficult challenge when working with delicate materials such as the 3D PCL scaffolds used here, as the plasma can completely destroy the scaffold or severely alter the morphology of the network. Figure 1a shows a photograph of an untreated scaffold (far right), along with two scaffolds that were treated in a 30 W N_2 plasma under non-optimized conditions (left). As can be seen, the plasma-treated scaffolds are significantly smaller than the untreated scaffold, with the polymeric network having collapsed during plasma processing. In addition, the tops of the scaffolds appear to be discolored, indicating the scaffolds were effectively "burned" by being in the plasma. This could come from energetic plasma species, but more likely the scaffolds suffered from ambient heating of the reactor walls. Such effects can be minimized by adding ceramic sleeves to the reactor, which will protect the substrates from any thermal energy given off by the reactor itself or by using a polymethylmethacrylate (PMMA) substrate holder in place of a glass slide. Nonetheless, causing severe damage to the scaffolds such as that shown in Figure 1a is a non-ideal situation that suggests careful optimization of plasma parameters is required for surface modification of 3D scaffolds.

Over the past two decades, much effort has been made to minimize damage to polymeric substrates in plasmas processing by the Fisher group and others. Effective strategies include limiting ion bombardment by the use of pulsed or rotating plasmas,[21,29,31−34] downstream or remote processing,[35] and constraining the parameter space to very low-power (3−10 W applied), low-pressure (<100 mTorr), and short-time (≤ 2 min) regimes.[36,37] Figure 1b shows a photograph of an untreated PCL scaffold (right), along with one that was treated downstream in a 50/50 NH_3/H_2O plasma (30 W, 4 min, 250 mTorr, left). Clearly, the plasma parameter space was much better optimized to minimize damage to the material, relative to the conditions used in Figure 1a. Indeed, the treated scaffold looks virtually identical to the untreated scaffold, indicating the scaffold network is intact and no physical damage has been imparted to the scaffold by energetic plasma species or from ambient heating of the glass walls. Further evidence of this is provided by SEM analysis, discussed below.

Water Contact Angle Measurements. As has been discussed in detail previously,[6,12,18,38] for many biomedical applications, tailoring the surface properties of biomaterials is critical to optimizing functionality. In particular, it has been shown that hydrophilic surfaces can be more conducive to the growth and proliferation of many cell types.[2−4,7,39] The primary manner in which hydrophilicity is measured is via WCA measurements. For flat surfaces, obtaining WCA data is relatively straightforward. For textured substrates, however, WCA measurements become more complicated as the measurement is affected by both surface chemistry and surface morphology.[40,41] Similarly, porous substrates such as the 3D PCL scaffolds discussed here present an even more challenging measurement and analysis situation. Not only can the surface of the scaffolds be relatively rough (in comparison to a silicon wafer, for example), but if the porous scaffold is rendered hydrophilic by plasma treatments, the water drop will rapidly spread and absorb into the scaffold matrix, sometimes too rapidly to accurately capture contact angle data. These effects make it difficult to derive meaningful contact angle data for our constructs[42] and understand differences in surface wettability imparted by different plasma treatments.

One way we and others have approached WCA measurements on porous substrates is to use a CA goniometer equipped with video capture.[20,43,44] This allows for measurement of both the contact angle and the drop volume as a function of time, thereby allowing the contact angle kinetics to be determined.[42] Figure 2 shows both WCA and drop volume data as a function of time for a PCL scaffold that was treated in a 30 W 50/50 H_2O/N_2 plasma for 4 min. Data taken immediately after treatment show the treatment has sufficiently modified the scaffold to allow complete absorption of the water drop to occur in ~20 ms. Moreover, the WCA (taken at t = 0 s, or ~100°) has significantly decreased from that of the untreated PCL scaffold (130 ± 5°, not shown) (see Figure 2a). Notably, a drop placed on the surface of untreated constructs does not absorb into the scaffold pores. Data taken one week after treatment on the same treated scaffold (Figure 2a) indicate that the material can still be considered to be more wettable, as the t = 0 WCA is still lower than that for the untreated scaffold and the water drop still disappears, although the time required for the drop to disappear has increased to ~180 ms. We have chosen to report the WCA at t = 0 because this time point can be considered a good representation of surface interactions (i.e., dependent on surface functionality), whereas WCA values at t > 0 may contain morphological contributions from the way the drop absorbs through the porous scaffold network.[42] The time it takes for the drop to disappear does, however, does provide a semi-quantitative approach to compare the effectiveness of different treatments and to assess the effects of aging on scaffold surfaces.

Alternatively, the change in drop volume as a function of time can be used to determine water absorption rates, which provides a complementary—and, perhaps, more direct and quantitative—comparison between treatments. Figure 2b shows the drop volume data that correspond to the WCA data shown in Figure 2a. Here, one of the challenges is accurately analyzing the data to provide the water absorption rate (expressed in units of μL/s). Thus, Figure 2b also shows both linear and cubic fits to two datasets: one taken immediately after plasma treatment with a 50/50 H_2O/N_2 plasma, and the other taken on a scaffold aged 1 week after treatment. Ideally, the volume data should decrease linearly with time, and the slope of a linear least squares regression analysis would provide effectively the average absorption rate, $\langle k_{ab} \rangle$, for a given sample if it accurately represented the entire dataset. If the line only fit the steepest tangents to the volume/time trace, but did not accurately reproduce the data over the entire time span, the fit would provide an initial absorption rate value, k_{iab}. Clearly, for the Figure 2b data acquired from the freshly treated sample, the linear least-squares approach provides an excellent fit to the entire dataset (R^2 = 0.99) and yields $\langle k_{ab} \rangle$ = 115 μL/s for this dataset.

As the samples age, it takes longer for the drop to adsorb, and the general shape of the curve may become nonlinear as there are more data points and the morphology (e.g., interconnectedness of the pores) of the sample may cause small plateaus in the drop volume data as a function of time, even if the drop is completely adsorbed by the scaffold. This is analogous to reaction rate data wherein the reaction under study is complicated by multiple (sequential) steps and/or side reactions that can also affect rate data. As can be seen from the data in Figure 2b for the 1-week-aged scaffold, a linear fit does not reproduce the data as well as it did for the freshly treated scaffold (R^2 = 0.95). Alternatively, the use of a third-order polynomial to fit the aged sample data provides a better fit and can account for variability in drop volume as a result of scaffold morphology (R^2 = 0.98). Note that this type of analysis, however, provides k_{iab}, rather than $\langle k_{ab} \rangle$. To directly compare the two fitting methods for the aged data shown in Figure 2b, the cubic fit yields k_{iab} = 16 μL/s, whereas the linear fit yields $\langle k_{ab} \rangle$ = 15 μL/s. For completeness, a cubic equation was also used to fit the data for the freshly treated scaffold; the results of this analysis gave a value of k_{iab} = 126 μL/s. Notably, the aged scaffold absorbs water at a much slower rate than the freshly treated scaffold, which is likely the result of hydrophobic recovery and/or surface oxidation upon exposure to atmosphere. This is discussed further in the next section, on surface compositional analysis.

Compositional Analysis. Several techniques can be used to provide compositional analysis of scaffolds, such as Fourier transform infrared spectroscopy (FTIR), XPS, and time-of-flight secondary ion mass spectrometry (ToF-SIMS). If what is desired is specific information on the scaffold surface, however, FTIR would provide the least amount of information, since IR spectroscopy has a penetration depth on the order of micrometers, even when used in total internal reflectance mode. Alternatively, ToF-SIMS is extremely surface-sensitive and thus could provide extremely detailed and spatially resolved compositional analysis. However, the topography encountered in our 3D architectures can induce artifacts in the ToF-SIMS data that are not easily resolved. Nevertheless, ToF-SIMS has been used to examine microspheres and other biomedically relevant constructs.[45,46] Here, we will focus on the use of the surface-sensitive technique of XPS for compositional analysis.

A range of plasma chemistries can be used to tailor the surface properties of biomaterials, depending on the needs of the end application. As noted above, hydrophilicity has been identified as being critical for many biomedical applications. In addition, several researchers have suggested that nitrogen functionalities can promote cell growth and proliferation.[18,47] Nitrogen can be implanted into PCL scaffolds using plasmas containing N_2 or NH_3, or can be incorporated via thin film deposition using a precursor such as allylamine,[27] or via plasma graft copolymerization using acrylamide as the polymerizing monomer.[11,15] However, there are several issues associated with plasma surface modification of 3D polymeric biomaterials, as well as the subsequent characterization of implanted functional groups. For example, with a porous material, it is important to ensure that the entire cross section be treated by the plasma. In the case of nitrogen-implanting plasmas, the effectiveness of the treatment can be monitored by measuring atomic concentrations of the top and cross sections of the scaffolds using XPS. Ideally, XPS measurements could be made at known depths along the cross section of a scaffold. Most XPS instruments have spot sizes that are on the millimeter scale, which makes such measurements challenging, but not impossible to perform on samples of the size used here (i.e., 10 or 20 mm × 3 mm).[11,15] Care must be taken to ensure accurate reporting of data acquired across the interior of a sectioned scaffold, especially if high spatial resolution of chemical composition data is desired. Perhaps more challenging, however, is the interpretation of the data acquired from such a cross-sectional analysis.

Figure 3 shows the nitrogen concentration found in PCL scaffolds treated in H_2O/NH_3 plasmas as a function of the NH_3 concentration in the feed. Data for the tops and cross sections of freshly treated scaffolds are shown along with data for

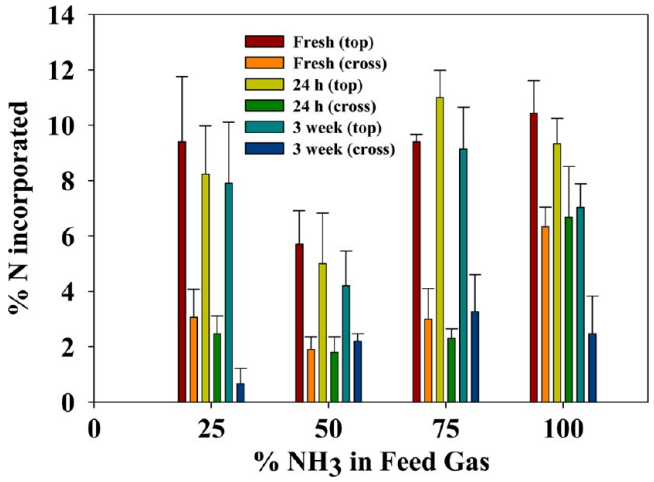

Figure 3. XPS atomic concentration of nitrogen incorporated into PCL scaffolds treated in NH_3/H_2O plasmas as a function of the NH_3 concentration in the feed gas. Data are shown for the tops (designated "top") and cross sections (designated "cross") of freshly treated, 24-h-aged, and 3-week-aged scaffolds. Error limits represent one standard deviation of the mean of several ($n \geq 3$) measurements made on each of multiple samples ($n \geq 2$).

scaffolds that have aged for 24 h and 3 weeks. Several observations can be made from these data. First, for all NH_3-containing plasmas, significant amounts of nitrogen are incorporated into the top of the scaffolds, with values ranging from ~6% to 10%. Second, we see a significant decrease in the amount of nitrogen incorporated into the scaffold cross section, with values ranging from 2% to 7%. Although it could be argued that limited diffusion of plasma species within the scaffold matrix is the cause of this decrease, it is also important to remember that, when the scaffolds are cut for cross-sectional analysis, large areas of untreated PCL are exposed. The XPS analysis thus includes significant contributions from untreated PCL. Given the high surface area of the scaffold cross section that can be attributed to untreated material, this undoubtedly accounts for the vast majority of the discrepancy in nitrogen content between scaffold tops and cross sections. Overall, it is also clear from the Figure 3 data that, for each plasma system, the nitrogen content of the scaffolds is extremely stable for the first 24 h, with slight decreases after 3 weeks. The most notable exception to this appears in the data for scaffolds treated in 100% NH_3 plasmas, wherein, after 3 weeks of aging, we see ~35% and ~60% decreases in nitrogen for the tops and cross sections, respectively.

Returning to the issues associated with compositional data collection and interpretation, it is important to also consider the issue of diffusion of active species through 3D biomaterial networks. We have previously demonstrated that surface modification species in NH_3/O_2 and H_2O plasmas effectively penetrate microporous polymer membranes, providing uniform surface modification of layers 50−500 μm thick.[20,43,44,48] Moreover, Jacobs et al. have demonstrated complete modification of a 6 mm × 3 mm PCL scaffold with 200−300 μm pores using an air plasma.[16] The scaffolds treated here are all 3-4 mm in thickness (10-20 mm in diameter), which could potentially push the boundaries for diffusion of active plasma species. Our results for both NH_3/H_2O plasmas as well as N_2/H_2O plasmas suggest, however, that the thickness of the scaffold is not a significant issue for surface modification/implantation systems. It could, however, be more of a concern for film deposition systems wherein active deposition

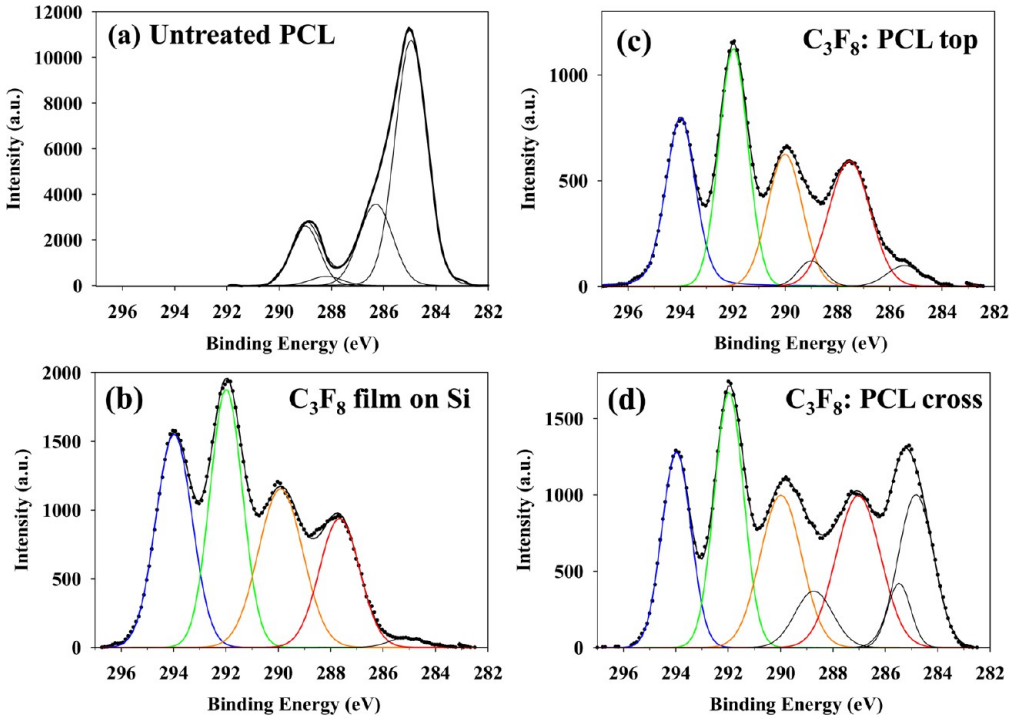

Figure 4. XPS C_{1s} high-resolution spectra for (a) an untreated PCL scaffold; (b) a fluorocarbon film deposited on a Si wafer in a C_3F_8 plasma; and (c) the top and (d) cross section of a PCL scaffold treated in a C_3F_8 plasma using identical treatment parameters. Conditions for the fluorocarbon plasma treatments were as follows: applied rf power, 50 W; operating pressure, 50 mTorr C_3F_8; treatment time, 20 min; and substrate location: 15 cm downstream from the coil. Note that, for comparison, the *x*-axes all span from 297 eV to 282 eV.

dx.doi.org/10.1021/am4025966 | ACS Appl. Mater. Interfaces 2013, 5, 9312−9321

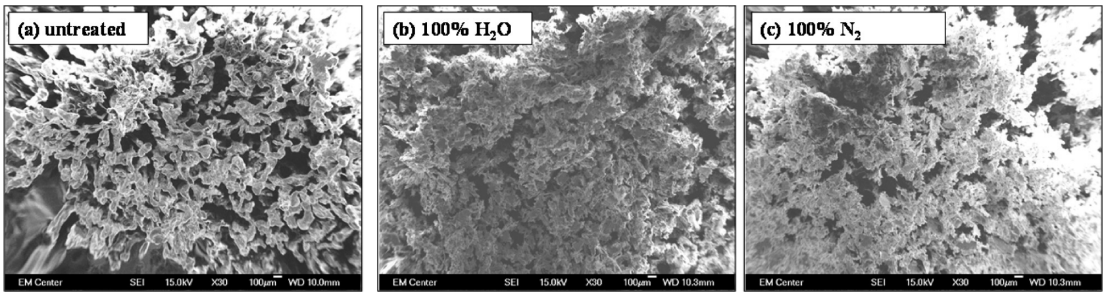

Figure 5. Scanning electron microscopy (SEM) images for PCL scaffold tops: (a) untreated, (b) treated in a 100% H_2O plasma, and (c) treated in a 100% N_2 plasma. These images are representative of images for scaffolds treated in all surface modification (functional group implantation) plasmas.

precursors, which may be larger molecular species, are key to film formation. Alexander and coworkers explored nitrogen incorporation into PD,LLA scaffolds via film deposition and plasma graft copolymerization systems, and they proposed that their inconsistent film deposition within the scaffold was the result of limited diffusion of film precursors within the 3D network.[11,15] Here, we used C_3F_8 plasmas, a well-studied film deposition system,[49,50] to demonstrate the challenges both in creating a robust, viable plasma deposition treatment for 3D biomaterials and in interpreting XPS data arising from these processes.

Figure 4 contains high-resolution C_{1s} XPS spectra for two control materials—untreated PCL and a fluorocarbon film deposited onto a flat Si wafer from a C_3F_8 plasma—along with spectra for the top and cross section of a PCL scaffold treated in the same C_3F_8 plasma. The expected binding environments are present in the spectrum of the untreated PCL (see Figure 4a), specifically the four primary peaks noted in the experimental section above.[15,17] Similarly, the film deposited on the Si wafer displays characteristics of an amorphous fluorocarbon polymer (see Figure 4b), with binding environments attributable to $-CF_3$ (294.0 eV), $-CF_2$ (292.1 eV), $-CF$ (~289.7), $-\underline{C}-CF_x$ (287.3 eV), and a very small contribution from C−C/C−H at 285.0 eV. The largest contributions arise from the $-CF_3$ and $-CF_2$ moieties, consistent with previous results from our laboratory.[49,50] The spectra for a PCL scaffold treated in a C_3F_8 plasma, however, display significant differences from the control film shown in Figure 4b. The spectrum for the top of the scaffold (Figure 4c) is very similar to that of the film deposited on the silicon wafer, with some notable differences. Primarily, the C−C/C−H peak at 285.0 eV is much larger than that for the flat film, and a sixth peak at ~289 eV is needed to accurately deconstruct the spectrum into individual components. Both of these relatively small binding environments can be attributed to the underlying PCL substrate, suggesting the thickness of the film deposited on the top of the scaffold is close to the sampling depth of the XPS (4−10 nm). Overall, however, there is little difference in the film composition, with the F/C ratio being 1.6 ± 0.1 for the flat film and 1.6 ± 0.4 for the film deposited on the top of the scaffold.

In contrast, the spectrum of the C_3F_8 plasma-treated scaffold cross section (Figure 4d) contains significantly more hydrocarbon components, with the C−C/C−H peak at 285 eV nearly as intense as the $-CF_3$ peak at 294 eV. The overall relationship of the three hydrocarbon peaks clearly mimics the spectrum in Figure 4a for untreated PCL, which is a strong indicator that we are sampling two types of materials simultaneously. This is consistent with the idea that when the scaffold is cut for cross-sectional analysis, we are exposing significant quantities of untreated PCL. Thus, with these data, it is difficult to definitively discern whether the observed differences are the result of the same film being deposited within the scaffold, but at a lower deposition rate, or if a very different film is being deposited. This latter hypothesis could be true if, for example, diffusion of key film precursors such as ions or large C_xF_y oligomers was preferentially lower (or higher) than that of others (e.g., CF, CF_2). Notably, preliminary results from deposition studies using different treatment times indicate that scaffolds treated for 90 min have the same F/C ratio on the top and in the cross section of these treated materials, within experimental error. The high-resolution spectrum for the cross section still reveals components attributable to the untreated, exposed PCL, but they are significantly diminished from that shown in Figure 4d.

As a final note regarding XPS analysis of 3D biomaterials, the effect of surface features (such as those introduced by the porous nature of the scaffolds used here) cannot be ignored. Indeed, the interpretation of XPS data acquired on surfaces with laterally inhomogeneous surfaces can be problematic, simply because of variations in XPS signals as a result of "shadowing".[51−53] This effect is especially problematic for angle-resolved XPS studies, but clearly also affects data acquired using a single analysis angle, as the problem arises particularly with larger analysis angles, as neighboring microstructures and nanostructures can shadow peak intensity.[54] This has been discussed and modeled in detail previously,[51−53] but for the purposes of the present work, it is important to note that such effects can introduce relatively large errors in the XPS analysis. Again, this adds a level of complexity to comparison of elemental composition data between scaffold exteriors and interiors, since observed differences may or may not be real, but rather simply the effects of surface feature shadowing.

Scanning Electron Microscopy (SEM) Imaging. In choosing a particular material for a specific biomedical application, chemical and physical properties are clearly important considerations. In addition, overall morphology and surface topography become important considerations in developing artificial materials that can constructively interact with biological molecules to create biomimetic systems such as with tissue regeneration. Although researchers have developed a host of methods to produce 3D polymeric scaffolds,[4,10,14,38] significant inconsistencies in the formation process (i.e., each scaffold can have a different morphology and surface topography) can ultimately lead to poor interactions with biological species and/or device failure. For scaffolds produced in the porogen-leaching method employed here, the molding process introduces two morphologically different faces: one

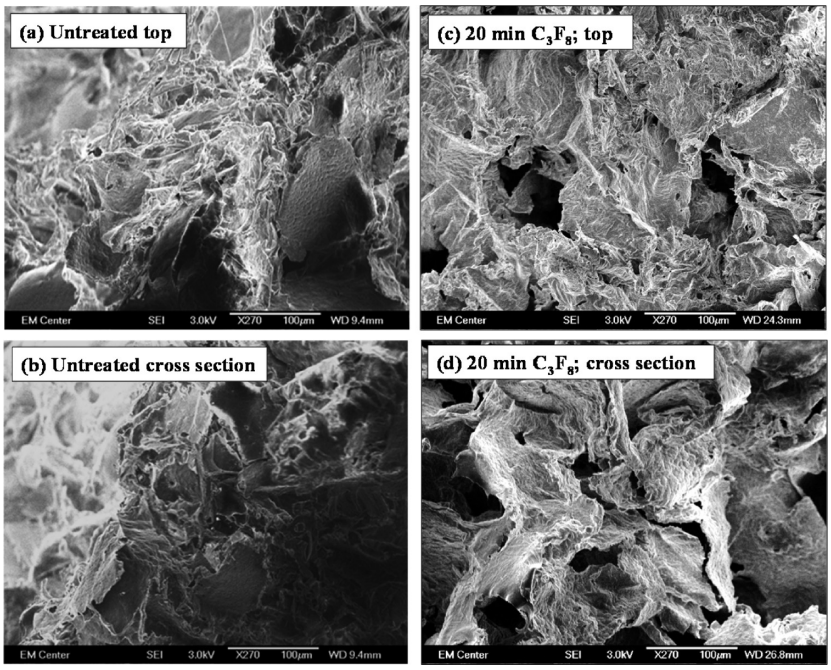

Figure 6. SEM images for PCL scaffolds: (a) untreated, top view; (b) untreated, cross-sectional view; (c) C_3F_8 plasma-treated, top view; and (d) C_3F_8 plasma-treated, cross-sectional view. Plasma treatments were performed using the same conditions as those given in the figure caption for Figure 4. These images are representative of images for scaffolds treated in all fluorocarbon plasma deposition systems.

that is in contact with the Teflon mold and the other that is in contact with air/ethanol/water during the curing process. Moreover, small changes in the porogen incorporation step can also lead to scaffold-to-scaffold differences in pore structure and geometry as well as interconnectedness. Morphological inconsistencies also exist with scaffolds produced in other methodologies, including solvent casting, electrospinning, emulsion, and freeze-drying as well as supercritical CO_2.[4,13,55] Plasma treatment of any of these materials could also introduce morphological changes either on the macroscopic scale, as demonstrated in Figure 1, or on the microscopic scale, potentially resulting in a breakdown of the polymer network.

Scanning electron microscopy (SEM) is used to evaluate morphological properties of 3D scaffolds, as well as any changes in morphology that may result from surface modification strategies such as plasma treatment. Figure 5 shows an SEM image of an untreated PCL scaffold along with representative images for scaffolds treated in 100% H_2O and 100% N_2 plasmas. These images show no major morphological differences between the untreated scaffold and the plasma-treated scaffolds. The pore structure remains intact, both on the top of the scaffold as well as within the interior of the scaffold. Indeed, for all optimized plasma surface modification systems that we have examined, none display any significant differences in scaffold morphology when examined by SEM, even at high magnification. This result is extremely promising for the use of plasmas to modify the surfaces of a range of porous polymeric biomaterials via functional group implantation.

With plasma polymerization systems, in addition to possible damage such as surface roughening, we run the risk of depositing a blanket-like coating on the top of the scaffold, effectively blocking the porous network.[23] Figure 6 contains higher-magnification SEM images of the top and cross section of an untreated PCL scaffold along with similar images of PCL scaffolds that have been treated in a C_3F_8 plasma for 20 min. As can be seen from these images, the nature of the porous network has not been changed appreciably. The pore structure is intact and the network appears to be conformally coated by the fluorocarbon film. As noted above, we have also treated scaffolds for 90 min in the C_3F_8 plasmas and the SEM images of these materials look virtually identical to those shown in Figure 6.

Two additional challenges with SEM analysis of our 3D scaffolds should be noted. First, as important as it is to examine the cross section of these materials to fully evaluate the surface modification, cutting the scaffold can introduce morphological changes. Indeed, care must be taken in the freezing and sectioning process to ensure that the scaffold is sufficiently "frozen", but not too cold, as the former situation can result in crushing of the network, whereas the latter can result in shattering of the scaffold during the cutting process. The second challenge is that these irregularly shaped polymer structures can experience intense surface charging during SEM analysis. Although this is of general concern with most soft materials, surface charging can usually be mitigated via sputtering a thin film (<5 nm) of a conducting material such as gold or chrome prior to analysis. Subjecting the scaffolds to the sputtering process, however, can damage or destroy the substrates and may also suffer from nonuniform coating, since sputtering is a line-of-sight coating method. The porous nature of the substrates are not conducive to effective coating via such methods. Thus, we have found it is better to not apply a conducting material to the scaffolds; instead, we employ relatively low accelerating voltages of ≤15 kV (usually ≤5 kV). Although signal intensity and image quality may decrease due to a decrease in the electron optical brightness at low accelerating voltages, the overall quality of the images is improved as surface charging is minimized.

Cell–Surface Studies. The viability of a particular material in a specific application such as tissue engineering largely rests on the ability of the material to encourage cell adhesion, proliferation, and differentiation into specific tissues. Two

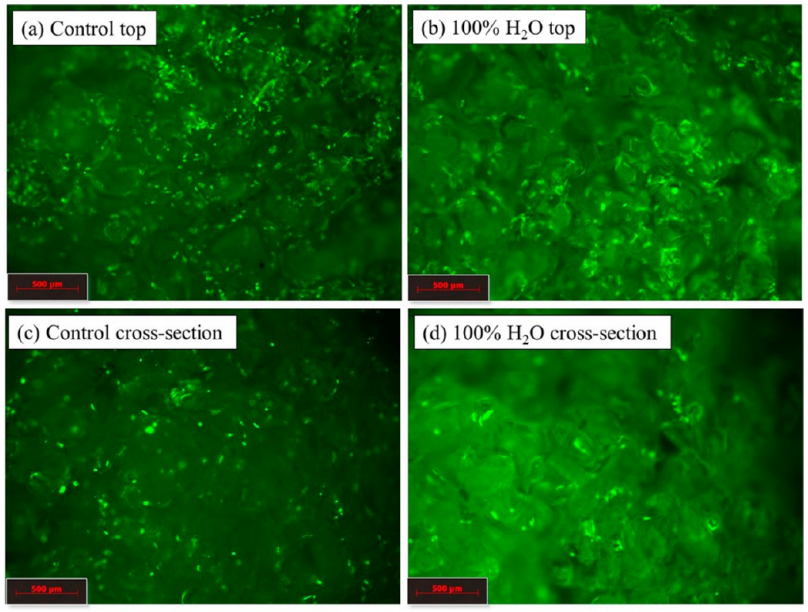

Figure 7. Fluorescence microscopy images of Soas-2 cells seeded on untreated and plasma-treated PCL scaffolds and incubated for 42 h. Panels (a) and (b) contain images of the top and cross section of the cells on an untreated scaffold, respectively, whereas panels (c) and (d) contain images of the top and cross section of the cells on a scaffold treated in a 100% H_2O plasma. These images are representative of images for all scaffolds treated in H_2O/N_2 plasma surface modification systems. The scale bar represents 500 microns.

bioassays were used to evaluate the efficacy of our H_2O/N_2 plasma treatments with respect to cell behavior. As detailed elsewhere,[27] metabolic activity was examined with the MTT colorimetric assay and results from this test suggest that there is little difference between untreated and treated scaffolds after 1 day of incubation. After 5 days of incubation, however, scaffolds treated in 100% H_2O, 50/50 H_2O/N_2, and 100% N_2 plasmas all showed enhanced cell growth over that on untreated scaffolds.[27]

Changes in cell morphology on different surfaces provides important information on material viability for biomedical applications. After ∼2 days of incubation after seeding scaffolds with Saos-2 osteoblast cells (Figure 7), fluorescence images indicate the cells largely exhibit a round morphology, with minimal surface area on the tops of untreated PCL scaffolds (see Figure 7a). This can indicate weak adhesion to the scaffold, and it suggests that the untreated material is not sending appropriate biological cues to the cells, which is consistent with previous studies.[11,12,17,19,56] In contrast, cells on 100% H_2O plasma-treated scaffolds are clustered (see Figure 7b) and exhibit a spreading morphology, including evidence of actin stress fibers. Spreading and the presence of stress fibers suggest that the cells are adhered to the substrate and respond to the topography. Similar results were obtained on scaffolds treated in 50/50 H_2O/N_2 and 100% N_2 plasmas, indicating that the cells preferred plasma-treated substrates over the untreated materials, regardless of plasma composition. This result suggests both nitrogen and oxygen functionalities imparted by plasma treatment are capable of enhancing cell growth for Saos-2 osteoblasts. Although beyond the scope of the current work, further experiments in our laboratory will focus on more detailed examination of the roles of different types of nitrogen functionalization in cell growth. Notably, fluorescence microscopy images of the cross sections of the scaffolds show cells penetrate the network and that the morphology of the cells within the interior of the scaffolds is very similar to that on the scaffold tops (see Figures 7c and 7d), which is further evidence that the plasma treatment affects the interior of the scaffold as well as the exterior surfaces.

As with other aspects of analysis of biomaterials, there are also numerous challenges associated with performing cell adhesion, growth, and proliferation studies on 3D scaffolds. Perhaps most obvious, the porosity and morphology of the substrate introduces an additional parameter (over flat substrates) that can significantly influence cell shape and adhesion. Thus, it can be difficult to separate effects arising from surface chemistry and those arising from topography or porosity. A second challenge is to achieve accurate analysis of cell morphology and differentiation throughout the interior of the 3D scaffolds. Indeed, images of the sections of the scaffolds suffered from high fluorescence background, possibly as a result of the porous nature of the scaffolds increasing scattering. Alternatively, the high background could be the result of autofluorescence of the polymer,[57] which can be substantial for polymers containing aromatic structures and/or conjugated backbones.[58] A final note on cell−surface interactions with respect to 3D scaffolds is that different cell lines may react differently to different plasma-treated materials.[39] In a recent review, Jacobs et al.[18] suggested that each combination of polymer, 3D structure, plasma treatment, surface functionality, and cell type represents an independent system. Although highly desirable, a comprehensive study that examined each of these parameters independently would be virtually untenable for any individual laboratory to undertake.

SUMMARY

In the arena of biomaterials, plasma surface modification and plasma deposition processes promise high flexibility for tuning the surface properties while maintaining the bulk properties of three-dimensional (3D) polymeric scaffolds. However, there are several challenges that must be addressed to ensure accurate evaluation and reporting of results from such surface

modification strategies. Thus, three major lessons and accompanying challenges discerned from the results presented here can be effectively summarized as follows. First, the plasma surface modification strategies described here clearly improve scaffold wettability via implantation of oxygen (H_2O-containing systems) and/or nitrogen functionality (NH_3 and N_2-containing systems). Upon treatment, the naturally hydrophobic poly(ε-caprolactone) (PCL) scaffolds were rendered extremely hydrophilic. More importantly, water absorption data also indicate that these treatments do not change appreciably over time, suggesting the materials do not undergo significant hydrophobic recovery. A major caveat to this, however, is that each process must be carefully optimized to avoid both macroscopic and microscopic damage to the delicate polymer network. Care must also be taken when analyzing and interpreting the dynamic contact angle data to derive water absorption rate information.

The second important result presented here is that functional group implantation plasmas (e.g., 100% H_2O, H_2O/N_2 or NH_3, and 100% N_2 or NH_3) are capable of modifying the entire cross section of relatively thick PCL scaffolds. Similarly, the fluorocarbon film deposition system using C_3F_8 plasmas also appears to penetrate the scaffold to deposit conformal coatings throughout the polymer network. Nevertheless, interfering signals attributable to contributions arising from the PCL scaffold exposed during scaffold sectioning complicate X-ray photoelectron spectroscopy (XPS) analysis of the treatment. It can also be challenging to accurately report cross-sectional composition data, since the spot size of XPS instruments can be large, relative to the total cross section. Finally, the surface chemistries resulting from the plasma surface modification systems used in this work are reliable enough to improve cell growth and proliferation over untreated materials. Cell response evaluation indicates the actin conformation of human Saos-2 osteoblast cells on plasma-treated scaffolds is significantly different than that on untreated scaffolds, and the morphology of the former is consistent with cells strongly adherent to the substrate. Challenges with cell−scaffold studies arise largely from scaffold porosity and the observation that different cell types are likely to interact with different surface chemistries very differently, thereby creating a somewhat unwieldy parameter space for plasma processing of 3D biomaterials. Nevertheless, the benefits of plasma processing suggest that additional research in this area could prove enormously fruitful, with important implications for numerous applications such as tissue engineering and regeneration, development of antimicrobial materials, and production of nonfouling surfaces. Thus, future directions in our laboratory include exploring alternate plasma systems and reactor designs, the use of alternate scaffold materials and architectures, and evaluation of the underlying chemical mechanisms involved in plasma processing of 3D polymeric constructs.

AUTHOR INFORMATION

Corresponding Author

*Tel.: 970 491 5250. Fax: 970 491 1801. E-mail: erfisher@lamar.colostate.edu.

Notes

The authors declare no competing financial interest.

ACKNOWLEDGMENTS

I thank my coworkers and collaborators Prof. Pietro Favia, Dr. Eloisa Sardella, Dr. Roberto Gristina, Dr. Jeffrey C. Shearer, Ms. Morgan E. Hawker, and Dr. Adoracion Pegalajar-Jurado for data collection and insightful discussions. Financial support for this work was provided by the National Science Foundation (No. CHE-1152963) and by the American Chemical Society Global Research Experiences, Exchanges and Training (GREET) program.

REFERENCES

(1) Higgins, M. J.; Molino, P. J.; Yue, Z.; Wallace, G. G. *Chem. Mater.* **2012**, *24*, 828−839.
(2) Pompe, T.; Keller, K.; Mothes, G.; Nitschke, M.; Tesse, M.; Zimmermann, R.; Werner, C. *Biomaterials* **2007**, *28*, 28−37.
(3) Rezwan, K.; Chen, Q. Z.; Blaker, J. J.; Boccaccini, A. R. *Biomaterials* **2006**, *27*, 3413−3431.
(4) Stevens, B.; Yang, Y.; Mohandas, A.; Stucker, B.; Nguyen, K. T. *J. Biomed. Mater. Res. B: Appl. Biomater.* **2008**, *85B*, 573−582.
(5) Pippa, N.; Merkouraki, M.; Pispas, S.; Demetzos, C. *Int. J. Pharmaceutics* **2013**, *450*, 1−10.
(6) Declercq, H. A.; Desmet, T.; Berneel, E. E. M.; Dubruel, P.; Cornelisson, M. J. *Acta Biomater.* **2013**, *9*, 7699−7708.
(7) Riedel, N. A.; Smith, B. S.; Williams, J. D.; Popat, K. C. *Mater. Sci. Eng. C* **2012**, *32*, 1196−1203.
(8) Hasan, J.; Crawford, R. J.; Ivanova, E. P. *Trends Biotechnol.* **2013**, *31*, 295−304.
(9) Wu, S.; Liu, X.; Yeung, A.; Yeung, K. W. K.; Kao, R. Y. T.; Wu, G.; Hu, T.; Xu, Z.; Chu, P. K. *ACS Appl. Mater. Interfaces* **2011**, *3*, 2851−2860.
(10) Woodruff, M. A.; Hutmacher, D. W. *Prog. Polym. Sci.* **2010**, *35*, 1217−1256.
(11) Barry, J. J. A.; Silva, M. M. C. G.; Shakesheff, K. M.; Howdle, S. M.; Alexander, M. R. *Adv. Funct. Mater* **2005**, *15*, 1134−1140.
(12) Domingos, M.; Intranuovo, F.; Gloria, A.; Gristina, R.; Ambrosio, L.; Bartolo, P. J.; Favia, P. *Acta Biomater.* **2013**, *9*, 5997−6005.
(13) Dorati, R.; Colonna, C.; Genta, I.; Modena, T.; Conti, B. *Polym. Degrad. Stability* **2010**, *95*, 694−710.
(14) Gong, X.; Tang, C. Y.; Wong, C. T.; Lu, W. W.; Zhang, Y.; Lam, W. M.; Wu, S.; Liu, J. *e-Polymers* **2010**, *10*, 1264−1272 (DOI: 10.1515/epoly.2010.10.1.1264, ISSN 1618-7229).
(15) Intranuovo, F.; Howard, D.; White, L. J.; Johal, R. K.; Ghaemmaghami, A. M.; Favia, P.; Howdle, S. M.; Shakesheff, K. M.; Alexander, M. R. *Acta Biomater.* **2011**, *7*, 3336−3344.
(16) Jacobs, T.; Morent, R.; De Geyter, N.; Desmet, T.; Dubruel, P.; Leys, C. *IEEE Trans. Plasma Sci.* **2011**, *39*, 2792−2793.
(17) Yildirim, E. D.; Besunder, R.; Pappas, D.; Allen, F.; Guceri, S.; Sun, W. *Biofabrication* **2010**, *2*, 014109 (12 pp).
(18) Jacobs, T.; Morent, R.; de Geyter, N.; Dubruel, P.; Leys, C. *Plasma Chem. Plasma Process.* **2012**, *32*, 1039−1073.
(19) Causa, F.; Battista, E.; Moglie, R. D.; Guarnieri, D.; Iannone, M.; Netti, P. A. *Langmuir* **2010**, *26*, 9875−84.
(20) Kull, K. R.; Steen, M. L.; Fisher, E. R. *J. Membr. Sci.* **2005**, *246*, 203−215.
(21) Malkov, G. S.; Fisher, E. R. *Plasma Process. Polym.* **2010**, *7*, 12.
(22) Malkov, G. S.; Martin, I. T.; Schwisow, W. B.; Chandler, J. P.; Wickes, B. T.; Gamble, L. J.; Castner, D. G.; Fisher, E. R. *Plasma Process. Polym.* **2008**, *5*, 129−145.
(23) Steen, M. L.; Flory, W. C.; Capps, N. E.; Fisher, E. R. *Chem. Mater.* **2001**, *13*, 2749−2752.
(24) Wavhal, D. S.; Fisher, E. R. *J. Membr. Sci.* **2002**, *209*, 255−269.
(25) Wavhal, D. S.; Fisher, E. R. *Langmuir* **2003**, *19*, 79−85.
(26) Yasuda, H. *Plasma Polymerization*; Academic Press: Orlando, FL, 1985.
(27) Shearer, J. C. Ph.D. Dissertation, Colorado State University, Fort Collins, CO, 2013.

(28) Bogart, K. H. A.; Dalleska, N. F.; Bogart, G. R.; Fisher, E. R. *J. Vac. Sci. Technol. A* **1995**, *13*, 476−480.
(29) Mackie, N. M.; Dalleska, N. F.; Castner, D. G.; Fisher, E. R. *Chem. Mater.* **1997**, *9*, 349−362.
(30) Mackie, N. M.; Castner, D. G.; Fisher, E. R. *Langmuir* **1998**, *14*, 1227−1235.
(31) Shearer, J. C.; Fisher, E. R. *Rev. Sci. Instrum.* **2013**, *84*, 063904.
(32) Leich, M. A.; Mackie, N. M.; Williams, K. L.; Fisher, E. R. *Macromolecules* **1998**, *31*, 7618−7626.
(33) McCurdy, P. R.; Truitt, J. M.; Fisher, E. R. *J. Vac. Sci. Technol. A* **1999**, *17*, 2475−2484.
(34) Bhattacharyya, D.; Pillai, K.; Chyan, O. M. R.; Tang, L.; Timmons, R. B. *Chem. Mater.* **2007**, *19*, 2222−2228.
(35) Butoi, C. I.; Mackie, N. M.; Gamble, L. J.; Castner, D. G.; Barnd, J.; Miller, A. M.; Fisher, E. R. *Chem. Mater.* **2000**, *12*, 2014−2024.
(36) Michelmore, A.; Martinek, P.; Sah, V.; Short, R. D.; Vasilev, K. *Plasma Process. Polym.* **2011**, *8*, 367−372.
(37) Gupta, B.; Krishnanand, K.; Dopura, B. L.; Atthoff, B. *J. Appl. Polym. Sci.* **2013**, *127*, 1744−1750.
(38) Chim, H.; Hutmacher, D. W.; Chou, A. M.; Oliveira, A. L.; Reis, R. L.; Lim, T. C.; Schantz, J.-T. *Int. J. Oral Maxillofac. Surg.* **2006**, *35*, 928−934.
(39) Godek, M. L.; Malkov, G. S.; Fisher, E. R.; Grainger, D. G. *Plasma Process. Polym.* **2006**, *3*, 485−497.
(40) Strobel, M.; Lyons, C. S. *Plasma Process. Polym.* **2011**, *8*, 8−13.
(41) Terriza, A.; Alvarez, R.; Yubero, F.; Borras, A.; Gonzalez-Elipe, A. R. *Plasma Process. Polym.* **2011**, *8*, 998−1002.
(42) Farris, S.; Introzzi, L.; Biagioni, P.; Holz, T.; Schiraldi, A.; Piergiovanni, L. *Langmuir* **2011**, *27*, 7563−7574.
(43) Steen, M. L.; Hymas, L.; Havey, E. D.; Capps, N. E.; Castner, D. G.; Fisher, E. R. *J. Membr. Sci.* **2001**, *188*, 97−114.
(44) Steen, M. L.; Jordan, A. C.; Fisher, E. R. *J. Membr. Sci.* **2002**, *204*, 341−357.
(45) Rafati, A.; Boussahel, A.; Shakesheff, K. M.; Shard, A. G.; Roberts, C. J.; Chen, X.; Scurr, D. J.; Rigby-Singleton, S.; Whiteside, P.; Alexander, M. R.; Davies, M. R. *J. Controlled Release* **2012**, *162*, 321−329.
(46) Desmet, T.; Poleunis, C.; Delcorte, A.; Dubruel, P. *J. Mater. Sci.: Mater. Med.* **2012**, *23*, 293−305.
(47) Park, H.; Lee, J. W.; Park, K. E.; Park, W. H.; Lee, K. Y. *Colloids Surf. B* **2010**, *77*, 90−95.
(48) Tompkins, B. D.; Dennison, J. M.; Fisher, E. R. *J. Membr. Sci.* **2013**, *428*, 576−588.
(49) Martin, I. T.; Malkov, G. S.; Butoi, C. I.; Fisher, E. R. *J. Vac. Sci. Technol. A* **2004**, *22*, 227−235.
(50) Cuddy, M. F.; Fisher, E. R. *ACS Appl. Mater. Interfaces* **2012**, *4*, 1733−1741.
(51) Artemenko, A.; Choukourov, A.; Slavinska, D.; Biederman, H. In *WES'09 Proceedings of Contributed Papers, Part III*, 2009; pp 175−181.
(52) Hajati, S.; Tougarrd, S. *Anal. Bioanal. Chem.* **2010**, *396*, 2741−2755.
(53) Oswald, S.; Oswald, F. *Surf. Interface Anal.* **2008**, *40*, 700−705.
(54) Zemek, J.; Olejnik, K.; Klapetek, P. *Surf. Sci.* **2008**, *602*, 1440−1446.
(55) Xiang, P.; Li, M.; Zhang, C.-Y.; Chen, D.-L.; Zhou, Z.-H. *Int. J. Biol. Macromol.* **2011**, *49*, 281−288.
(56) Di Mundo, R.; Nardulli, M.; Milella, A.; Favia, P.; d'Agostino, R.; Gristina, R. *Langmuir* **2011**, *27*, 4914−4921.
(57) Mishra, G.; Easton, C. D.; Fowler, G. J. S.; McArthur, S. L. *Polymer* **2011**, *52*, 1882−1890.
(58) Shadpour, H.; Musyimi, H.; Chen, J.; Soper, S. A. *J. Chromatogr. A* **2006**, *1111*, 238−251.